Applied Ocean Research 65 (2017) 290–301

Contents lists available at ScienceDirect

Applied Ocean Research

journal homepage: www.elsevier.com/locate/apor

Experiments with flexible shrouds to reduce the vortex-induced vibration of a cylinder with low mass and damping

M.M. Cicolin, G.R.S. Assi*,[1]

Department of Naval Architecture & Ocean Engineering, EPUSP, University of São Paulo, São Paulo, SP, Brazil

ARTICLE INFO

Article history:
Received 23 December 2016
Accepted 3 April 2017
Available online 9 May 2017

Keywords:
Vortex-induced vibration
Suppression
Flexible shroud
Drag reduction
Ventilated trousers

ABSTRACT

Experiments employing a low-mass-damping cylinder have been conducted to determine the vortex-induced vibration (VIV) response of four suppressors of the flexible-shroud family. The VIV suppressors were inspired in the concept of the *Ventilated Trousers* (VT), a flexible shroud composed of a flexible net fitted with three-dimensional bobbins. Reynolds number varied between 5×10^3 and 25×10^3, while reduced velocity varied from 2 to 26. The VIV dynamic response showed that the VT suppressed the peak amplitude of vibration down to 40% of that of a bare cylinder. Other flexible shrouds also achieved suppression, but not as efficiently. Drag was reduced during the VIV synchronization range, but remained above the value for a bare static cylinder thereafter. Spectral analysis of displacement and lift revealed that, depending on the geometry and distribution of the bobbins, the flexible shroud can develop an unstable behavior, capturing energy from the wake and sustaining vibrations for higher reduced velocities. PIV measurements of the wake revealed that the entrainment flow through the mesh is necessary to extend the vortex-formation length of the wake; this mechanism only occurs for the VT mesh.

1. Introduction

The vibration induced by the external flow past slender structures poses a problem to submarine and offshore cables, flexible pipes, drilling and production risers and other elastic structures exposed to sea currents. The excitation has its origin in the shedding mechanism of alternating vortices occurring in the wake of bluff bodies, so the hydroelastic phenomenon is called vortex-induced vibration (VIV). Flexible lines exposed to vibrations for a long time may be damaged by structural fatigue [1]. The amplification of drag due to the vibration of the body is also of considerable concern, since it increases static and dynamic loads at the joints, platform and other fixtures.

One way to mitigate the effects of VIV is the installation of suppressors along the riser, or at least on the length of the line where currents are most intense. Helical strakes and fairings, for example, have been widely employed by the industry as VIV suppressors [2]. On one hand, significant VIV suppression of light structures requires wider strakes, which increases drag. Fairings, on the other hand, tend to be more efficient in suppression as far as drag is concerned, but may suffer from hydroelastic instabilities [3]. With the improvement of molded plastic, helical strakes and fairings have indeed become sturdy contraptions, but they still take considerable time to install and occupy large areas on the deck. Other devices based on the disruption of the wake by interfering control surfaces (as explored by Silva-Ortega and Assi [4], for example) may suffer from the same problem.

During the last decades many devices have been investigated and offered as commercial products. Following the industry demand for more efficient, robust and easy-to-install devices, the technological development for suppressing VIV has been under pursuit by both the scientific and industrial communities.

In this context, All Brown Universal Components, a technology company based in the UK, created an interesting new device for suppressing VIV of drilling risers called the *Ventilated Trousers*, or simply VT [5]. Composed of a net of flexible cables holding an orthogonal array of bobbins (solid elements fitted on the net), the VT suppressor is, in the words of the inventors, "a loose fitting sleeve in the form of a light flexible net with integral bobbins in a special arrangement. It is omni-directional, rugged, and made from materials compatible with the offshore environment" [6]. Essentially, the VT is an improvement on the idea of wrapping the drilling riser in a type of flexible cover able to deform with the flow, interact with the wake and mitigate the response to hydrodynamic loads.

* Corresponding author.
E-mail address: g.assi@usp.br (G.R.S. Assi).
[1] Currently a Visiting Associate in Aerospace at GALCIT, California Institute of Technology.

http://dx.doi.org/10.1016/j.apor.2017.04.003
0141-1187/

The suppression effectiveness of the VT and its efficiency concerning drag reduction have been studied over the last years with promising results [7,6,8]. Brown and King [7], for example, performed experiments in a laboratory scale with flexible cylinders showing a 90% reduction of the VIV peak amplitude of displacement at a Reynolds number (Re) of approximately 1.4×10^5. So far, all known experiments have been performed either with flexible pipes or near real conditions at sea, especially regarding the range $Re = 3.7 \times 10^4$ to 1.2×10^6 and the structural properties of a riser [7,6]. Although this kind of experiment verifies the potential of such a device in practical applications (for being performed closer to real conditions), they are not designed to reveal the intricate hydrodynamic mechanisms by which the VT is able to achieve suppression.

1.1. Objective

In the present work we set out to understand the behavior of the VT and other similar suppressors in idealized laboratory conditions. It could be said that the VT is part of a larger family of suppressors, here called the *flexible shrouds* (also called *permeable meshes* in our previous investigations). We believe that exploring geometric variations based on the VT concept will produce siblings that could thus reveal the fundamental physical mechanisms behind the suppression.

Purely motivated by the scientific interest on the topic, the present work is part of an investigation to study the behavior of this family of suppressors at moderate Re, low mass and very low damping conditions. We are particularly concerned with the scientific investigation of the hydrodynamic and hydroelastic mechanisms that will explain us how this family of VIV suppressors works.

We will characterize the VIV response of the VT and three other simpler flexible shrouds derived from it. In idealized laboratory conditions all variables are under control and crucial parameters are reduced to enhance the response. The idea is to test the suppression device in the most undisturbed condition, indeed different for the real application in the ocean, but free from most of the interference that could mask the understanding of the fundamental physical phenomena. As will become clearer shortly, the differences between the models emerge from variations on the geometric parameters of the original VT, taking us step by step in understanding the physical principles.

2. Experimental method

Experiments have been carried out in the recirculating water channel of NDF Fluids and Dynamics Research Group at the University of São Paulo, Brazil. The water channel has a test section 0.7 m wide, 0.9 m deep and 7.5 m long. The flow speed (U) is variable up to 1 m/s, allowing for tests with different values of Reynolds number, with a turbulence intensity of less than 3%.

Models were attached to a one-degree-of-freedom rig which allowed the model to oscillate freely in the cross-flow direction (y), as shown in Fig. 1. The platform was mounted on air bearings to reduce friction within the system, thus ensuring very low structural damping and maximum response. A load cell installed between the cylinder and the rig measured instantaneous lift and drag forces acting on the cylinder. A pair of coil springs provided the restoration force to the system and an optical sensor measured the displacement without adding extra damping. For further details on the elastic rig, other VIV experiments employing the rig and information on the facilities please refer to [9,10].

Tests were performed with a rigid section of a circular cylinder (external diameter $D = 50$ mm, submerged length $L = 650$ mm) fitted with four different flexible shrouds. Variations of the meshes

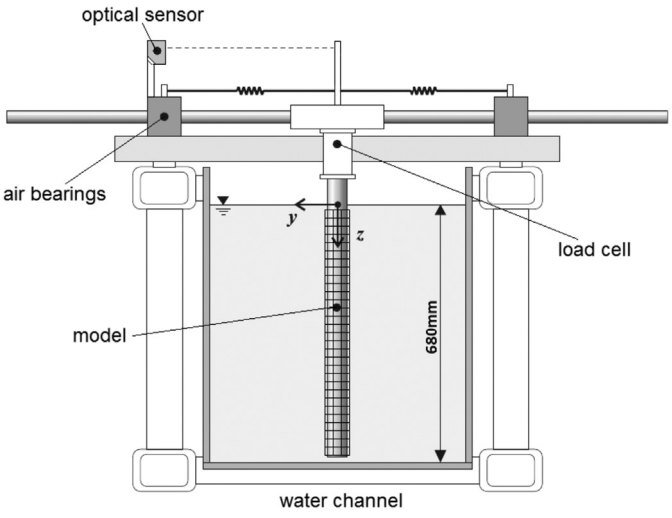

Fig. 1. Cross-view of the test section showing the elastic rig and cylinder in the water channel.

concerned the geometry of the bobbins, focusing on the main length scales of the original bobbin, and their distribution on the net.

The first model is a pure reproduction of the VT device. Its main properties are the perimeter (p), the width of the mesh element (w) and a characteristic dimension of the bobbin (d), as can be seen in Fig. 2. Brown [5] provides a guide for the geometric definition of the mesh, allowing some variations on its properties: the diameter ratio, for example, must vary between $d/D = 0.08$ and 0.125. Besides that, in a previous work, Brown and King [7] verified that a mesh element width of 5 times the bobbin characteristic dimension ($w = 5d$) resulted in a more effective VT than one in which $w = 3d$. They also reported that the net perimeter must be between $p = 4D$ and $4.71D$. Following these guidelines and considering that the parameters are not completely independent, the largest possible mesh was built respecting the restrictions and recommendations proposed by Brown [5]. The final dimensions of the VT model employed in the present work are shown in Table 1.

Based on the VT mesh, presented in Fig. 3a, three other meshes with simpler geometries have been built altering the VT bobbin geometry and distribution, but keeping the same w and p. The *thick-sparse mesh*, shown in Fig. 3b, had different bobbins formed by only one circular cylinder with an external diameter of $d_{ext} = 3d$, corresponding to the outer diameter of the VT bobbin. On the other hand, the bobbin of the *thin-sparse mesh* shown in Fig. 3c, was made with a single cylinder with external diameter $d_{ext} = d$, resulting in a mesh following the thinner elements of the VT bobbin.

The VT, the thick-sparse and the thin-sparse meshes all had the same bobbin distribution, with bobbins fitted on every other mesh element. Now, the third variation resulted in the *thin-dense mesh* shown in Fig. 3d. It was built with the same bobbins used in the thin-sparse mesh, but fitting bobbins in every element of the net, resulting in a different distribution of bobbins.

In summary, all three bobbins have the same height of $5d$, but they vary in shape and how they are distributed on the mesh, as illustrated in Fig. 3 and Table 1. Again, all new bobbins are based on the main length scales found in the VT bobbin: height $5d$ and diameters d or $3d$.

By keeping the net perimeter (p) constant for all meshes and varying the outer diameter of the bobbins, the thin meshes presented a loose fit around the cylinder when compared with the other two. At first, this was not intentional, since we believed that keeping p constant would support the direct comparison of the results. However, as will be discussed later, the loose meshes had quite a significant and interesting effect in the response.

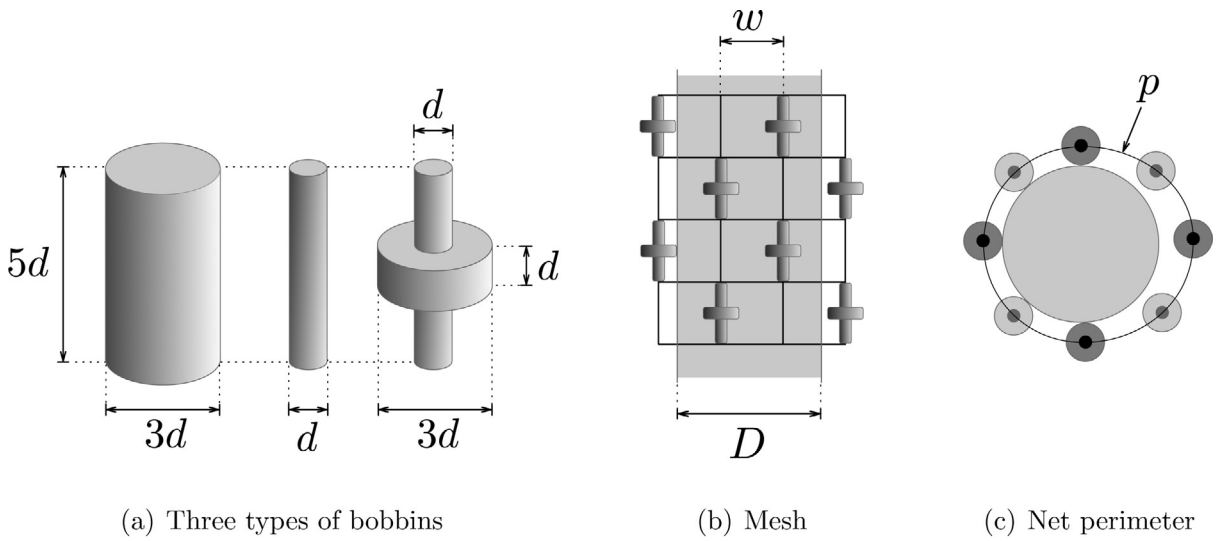

Fig. 2. Geometric properties and dimensions. (a) Three types of bobbins: thick cylinder, thin cylinder and VT bobbin. (b) Mesh distribution. (c) Net perimeter.

Table 1
Model properties.

Model	Bobbin	Distribution	d	(mm)	d_{ext}	w	p
VT mesh	VT bobbin	Skip one cell	0.11D	(5.8)	3d	5d	4.64D
Thick-sparse mesh	Thick cyl.	Skip one cell	0.11D	(5.8)	3d	5d	4.64D
Thin-sparse mesh	Thin cyl.	Skip one cell	0.11D	(5.8)	d	5d	4.64D
Thin-dense mesh	Thin cyl.	Every cell	0.11D	(5.8)	d	5d	4.64D

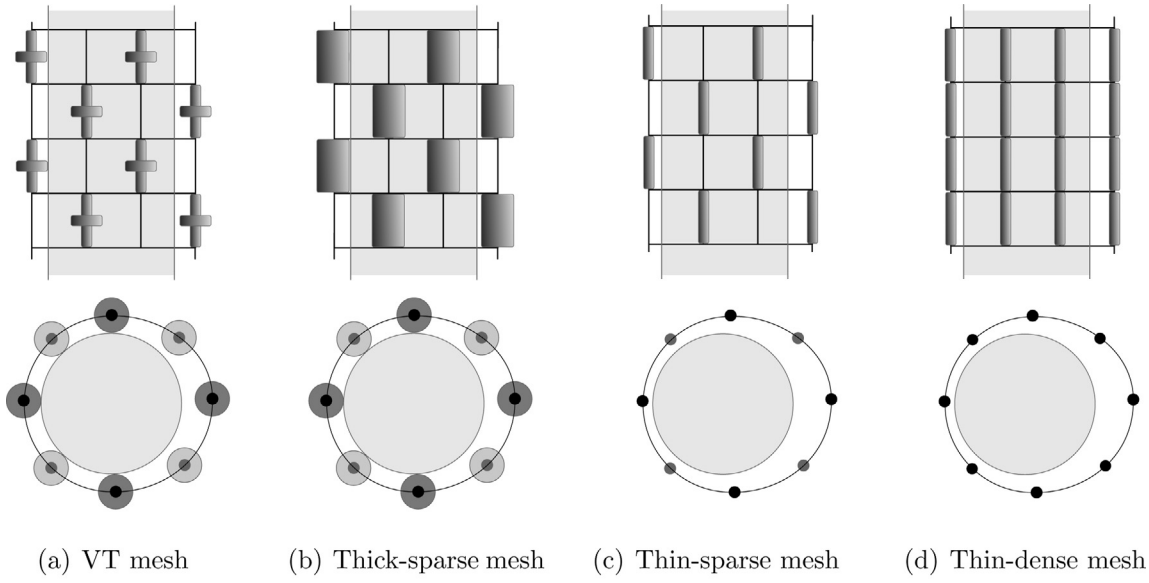

Fig. 3. Different configurations of the flexible shrouds. (a) VT mesh. (b) Thick-sparse mesh. (c) Thin-sparse mesh. (d) Thin-dense mesh.

3. Results and discussion

3.1. Preliminary results with static models

Preliminary experiments with fixed models have been performed as a reference for the hydrodynamic loads on a static body. The models were attached to the load cell on a fixed rig while measurements of drag and lift were taken. Hydrodynamic loads are presented in terms of force coefficients per unit length of cylinder, i.e. dividing lift and drag by $\frac{1}{2}\rho DU^2$, where ρ is the density of water and U is the free stream velocity.

Fig. 4a presents the mean drag ($\bar{C}_D$) and mean lift ($\bar{C}_L$) coefficients versus Re for all meshes compared with those for a bare cylinder. The bare cylinder presented $\bar{C}_D \approx 1.15$, which is in agreement with the results found in the literature for this range of Re [11,12]. All the meshes increased $\bar{C}_D$ when compared to that of the bare cylinder: an approximate increase of 30% for the VT mesh, 65% for the thick-sparse mesh, 40% for the thin-sparse mesh and 60% for the thin-dense mesh. Since drag was increased, the shrouds must increase the amount of kinetic energy lost to the wake. All flexible shrouds not only enlarge the frontal area exposed to the flow but also increase the kinetic loss due

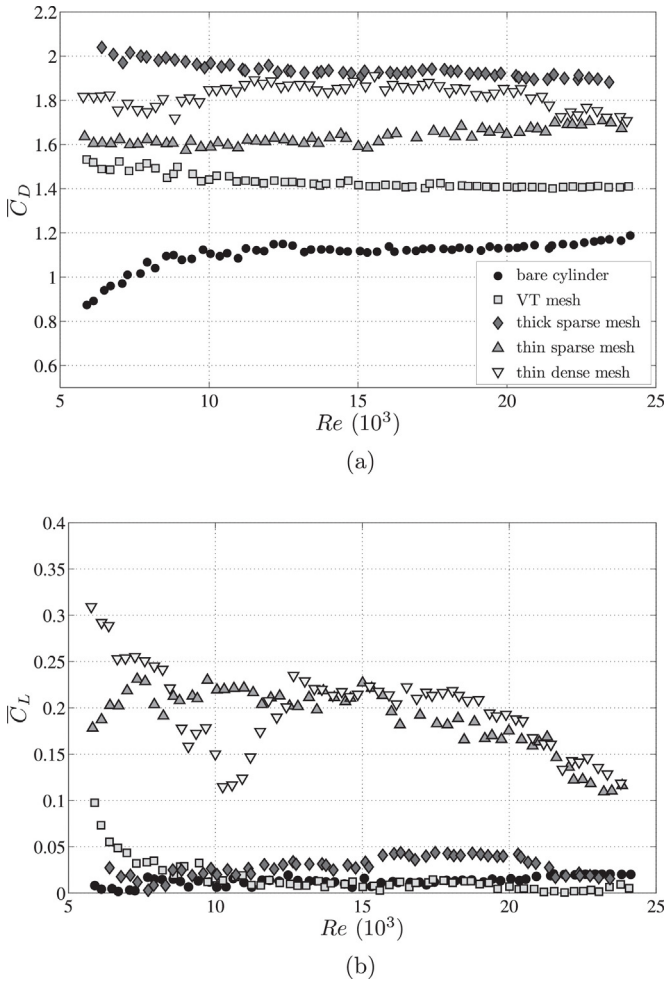

Fig. 4. Coefficients of (a) mean drag and (b) mean lift for static models versus *Re*.

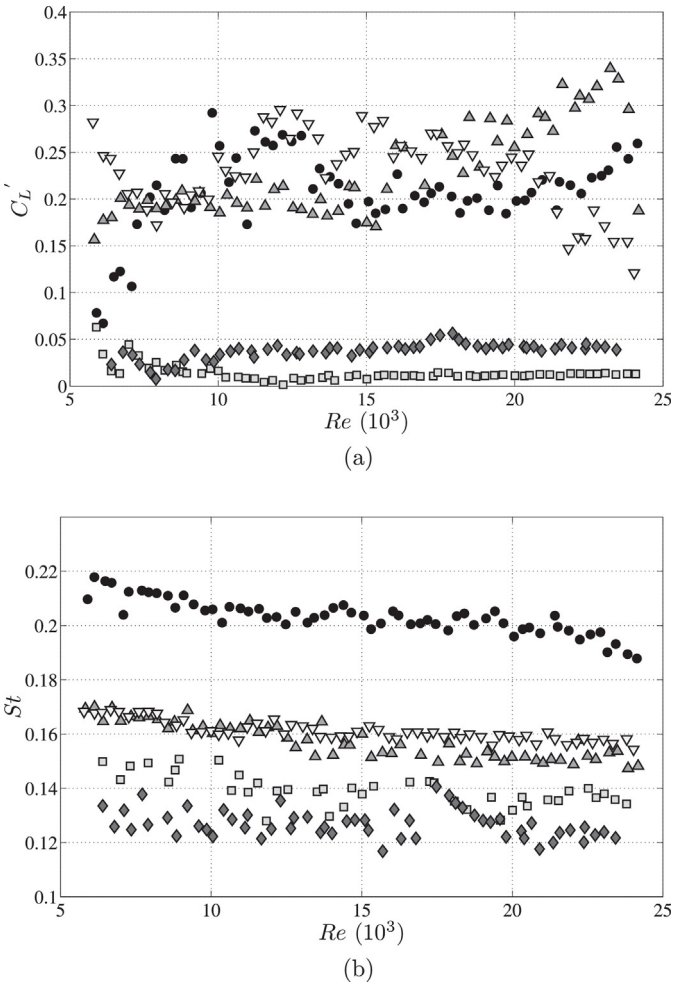

Fig. 5. (a) RMS of lift coefficient and (b) Strouhal number for static models versus *Re*. Key: please refer to Fig. 4.

to friction and locally-separated flow around the bobbins and net.

The mean lift coefficients presented in Fig. 4b, however, tell an interesting story. While the VT and the thick-sparse mesh have shown $\bar{C}_L$ very close to zero (and also the bare cylinder, as expected for symmetric bodies), the thin-sparse and the thin-dense meshes presented $\bar{C}_L$ distinctly higher for most of the *Re* range. It must be pointed out that even though the system (cylinder and load cell) was kept fixed, the flexible meshes were able to wobble around the cylinder responding to the unsteady flow. Because the VT and the thick-sparse mesh were tighter around the cylinder (compared to the other two loose meshes) they remained fairly static, while the thin meshes had more room to oscillate. Even though all meshes had the same perimeter, the larger size of the bobbins reduced the clearance between the devices and the main cylinder.

Now, both loose meshes tended to accommodate towards one of the sides of the cylinder, creating an effective asymmetry of the body, hence producing a residual mean lift. The meshes could randomly find stable positions on either side of the cylinder (in a kind of bifurcation), generating steady lift to either side. A very similar mechanism has been reported by Assi et al. [13] when investigating the dynamics of a cylinder fitted with free-to-rotate splitter plates. Of course in the present case the interfering body is not a solid plate, but a loose, flexible shroud interacting within the vortex formation region of the wake.

Fig. 5a presents the fluctuation of lift (C_L'), calculated as the RMS (root mean square) of the lift signal. The reference case for the bare cylinder shows a scatter of points around $C_L' = 0.2$, as expected for this *Re* range and in agreement with Williamson [14]. Similar to the mean lift discussed above, C_L' also reveals a different behavior for the thin meshes, with the same level of C_L' as that of the bare cylinder. This fluctuation is generated by the loose meshes oscillating towards one of the sides of the cylinder. The VT and the thick-sparse mesh, however, present very low C_L', showing that they might be effectively disrupting the vortex shedding mechanism in the near wake region.

The Strouhal number ($St = f_s D/U$, where f_s is the frequency of vortex shedding) was estimated from the frequency of fluctuation of the lift signal and is presented in Fig. 5b. As expected, the bare cylinder shows a typical value close to $St = 0.2$, in agreement with Norberg [15] for this range of *Re*. All meshes presented lower Strouhal numbers when compared to the bare cylinder, which means that their vortex-shedding frequencies are smaller due to a wider wake or a wake with weaker vortices.

Flow separation for these models is made very complex by the three-dimensional interference of the shrouds. Separation might be occurring from the various regions of the bobbins, from the cables of the net and ultimately from the wall of the main cylinder. The actual distance between the separated shear layers (to define the characteristic length in *St*) is not so clear, therefore we chose to non-dimensionalize *St* by the external diameter of the main cylinder (*D*). Now, the flexible shrouds are indeed enlarging the effective diameter of the body, but it is interesting to note that the thick-sparse mesh produced the lowest *St* (or shedding frequency) of them all. If the effective external diameter of the body were to

Table 2
Dynamic properties for the VIV series.

Model	m^*	First VIV series				Second VIV series			
		$f_{N_{air}}$	f_N	ζ_{air}	ζ_{water}	$f_{N_{air}}$	f_N	ζ_{air}	ζ_{water}
Bare cylinder	2.8	0.67	0.58	0.3%	1.6%	0.40	0.35	0.6%	2.0%
VT mesh	2.9	0.66	0.55	0.3%	6.0%	0.39	0.33	0.6%	7.5%
Thick-sparse mesh	2.9	0.67	0.50	0.3%	10.6%	0.39	0.31	0.6%	12.0%
Thin-sparse mesh	2.8	0.67	0.57	0.4%	3.6%	0.41	0.33	0.6%	6.1%
Thin-dense mesh	2.8	0.67	0.58	0.4%	4.0%	0.39	0.33	0.6%	8.8%

be approximated, say by adding the size of the bobbins to D, then the true value of St would be very close to 0.2 for all cases.

3.2. VIV response

Tests to determine the VIV response for the models were carried out by installing the cylinders on the elastic rig, which allow for free vibrations only in the cross-flow direction (y). The pair of coil springs that conferred the stiffness to the system was changed twice, resulting in two ranges of reduced velocity (U/f_ND) covering the same Re range. Thus the experimental results are divided in two series.

Table 2 presents the main structural properties for both series. The reduced mass (m^*, defined as the ratio of structural mass to the mass of displaced fluid) was approximately 2.9 for all models, which is close to the values found in real offshore applications. Free-decay tests were performed in air in order to determine the natural frequency ($f_{N_{air}}$) and the structural damping of the system (ζ_{air}, defined as a percentage of the critical damping). Additional decay tests performed in still water yielded the natural frequencies in water (f_N) and the total (structural plus hydrodynamic) damping (ζ_{water}) of the system. The reduced velocity was normalized using the natural frequency measured in still water (f_N).

3.2.1. First VIV series: reduced velocity up to 16

Fig. 6 presents the VIV response of all models with flexible shrouds compared with that of the bare cylinder as a reference. The displacement curve ($\hat{y}/D$, where $\hat{y}$ is calculated as the RMS of the displacement signal multiplied by $\sqrt{2}$) shown in Fig. 6a reveals the typical VIV response for the bare cylinder, with the initial, upper and lower branches of vibration clearly identified for a low-$m^*\zeta$ system. A peak amplitude of $\hat{y}/D \approx 0.9$ is found around reduced velocity 5, with synchronization occurring roughly between $U/(f_ND) = 4.5$ and 11.5. Within this range, the frequency of oscillation (f, calculated from the spectrum of displacement) is synchronized with the frequency of vortex shedding and both remain very close to the natural frequency of the system, as presented in Fig. 6b. Also for the bare cylinder, Fig. 6c highlights the amplification of mean drag, reaching a maximum of $\bar{C}_D \approx 3.1$, occurring in the synchronization range. Past reduced velocity 12, $\bar{C}_D$ returns to the value for a fixed cylinder of approximately 1.1, as the cylinder stops responding to VIV. Reference results for the bare cylinder are in good agreement with Williamson and Govardhan [16].

Now we shall turn to the VIV response of the cylinder fitted with the flexible shrouds. In general, Fig. 6a shows that all meshes managed to reduce the peak amplitude of displacement within the synchronization range. The VT reached a maximum amplitude of $\hat{y}/D \approx 0.38$, accounting for a 60% reduction when compared to the peak amplitude of the bare cylinder. The synchronization range has also been shortened by the VT. The frequency signature of the response, shown in Fig. 6b, is not much different from that observed for the bare cylinder. Peak $\bar{C}_D$, on the other hand, presented a 30% reduction during the synchronization range, but remained slightly higher ($\bar{C}_D \approx 1.45$) than that of the static bare cylinder by the end of the experiment. That is to say that the VT indeed suppresses

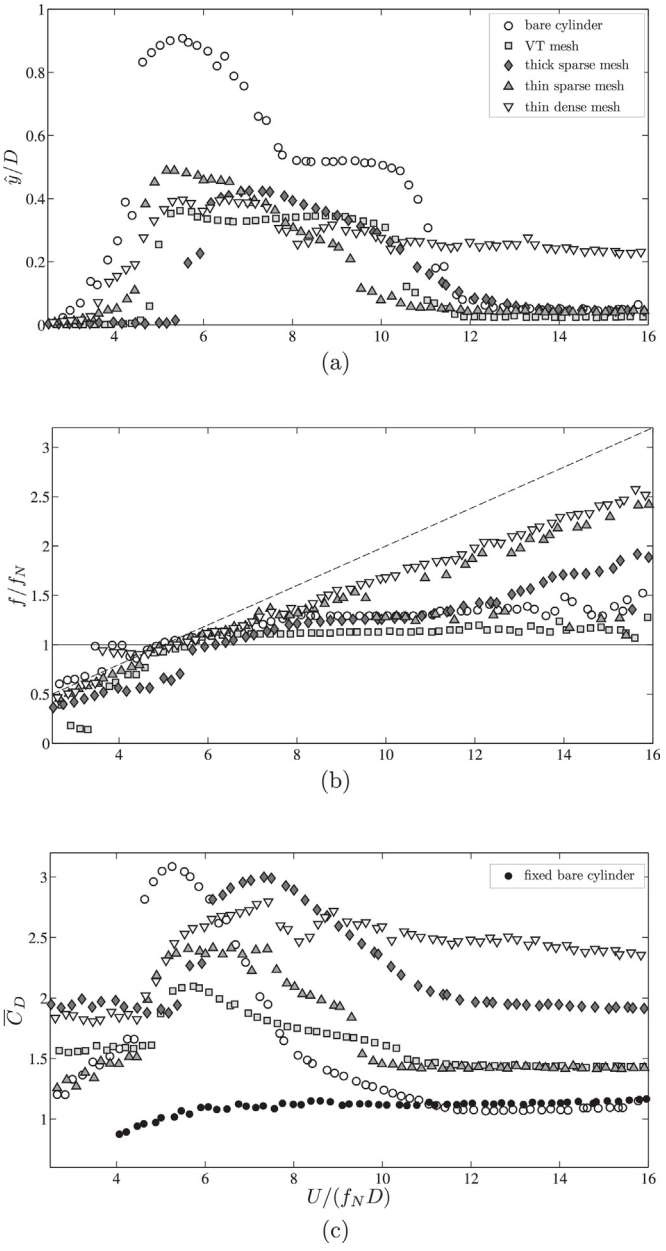

Fig. 6. Dynamic response of VIV versus reduced velocity: (a) amplitude of displacement, (b) dominant frequency of oscillation and (c) mean drag coefficient.

VIV and reduces the maximum drag amplified by the vibration, but once the vibration ceases, after the synchronization, the mean drag is higher than that of a bare cylinder.

The thick-sparse mesh follows the trend of VT, but is not as successful in reducing the peak amplitude of displacement. The response peak is shifted as the whole synchronization range is delayed in relation to the bare cylinder, starting at $U/(f_ND) = 5.5$ and

ending at 12. This is due to a significant increase in the effective diameter of the body, caused by the larger diameter of the bobbins. The maximum mean drag is almost as high as that of the bare cylinder during synchronization, but it remains approximately 70% higher once the vibration terminates. Again, this might be due to the enlarged size of the bobbins. The frequency signature is very similar to the other two previous cases.

The thin-sparse mesh follows the same behavior, reaching the highest peak of displacement of all the flexible shrouds (only a 40% reduction compared to the bare cylinder). The synchronization range is not dislocated to higher reduced velocities since the smaller size of the bobbins tend not the enlarge much the effective diameter of the body. The frequency response, however, shows a different behavior from the previous cases, with the dominant frequency of oscillation following just under the frequency of vortex shedding for the whole range of reduced velocity (the inclined dashed line in Fig. 6b corresponds to $St = 0.2$). $\bar{C}_D$ is reduced during the synchronization, but remains higher than that of a bare static cylinder when no vibration exists.

Finally, the thin-dense mesh shows the most interesting behavior of them all. While the peak displacement shows the same level as that for the VT during synchronization, the vibration does not die out as expected after resonance. For higher reduced velocities a steady value of $\hat{y}/D > 0.2$ is sustained until the end of the experiment. The frequency of response shows that the cylinder with a thin-dense mesh is persistently oscillating at the vortex-shedding frequency for the whole range of reduced velocities. As a consequence, the mean drag coefficient is also sustained at $\bar{C}_D \approx 2.5$ until the end of the experiment, while all the other models returned to their values obtained during the static-models experiments (Fig. 4).

The thin-dense mesh is able to capture energy from the vortex shedding mechanism, sustaining considerable vibration at the shedding frequency beyond the VIV synchronization. In fact, looking at the mesh during the experiments, we were able to note that the loose thin-dense mesh could wobble from side to side as the cylinder oscillated. The thin-sparse mesh would be as loose around the cylinder as the thin-dense mesh, but the latter was less permeable to the flow and able to interact with the unsteady wake. The concentration of bobbins on the thin-dense mesh together with its loose fit around the cylinder helped it to work as a sail, oscillating with the body (including a visible phase lag in the movement), interacting with the wake and thus exciting the cylinder into sustained oscillations.

Due to the distinct frequency response of the thin meshes, and especially due to the displacement response of the thin-dense mesh, we were motivated to extend the VIV experiments into a second series, this time changing to a softer set of springs to allow for higher reduced velocities (Table 2).

3.2.2. *Second VIV series: reduced velocity up to 26*

The results for the second VIV series will concentrate on the frequency signature of the response and the excitation, therefore we will be looking at the frequency signature of both displacement and lift.

The typical displacement response for the bare cylinder is shown again in Fig. 7, this time for reduced velocities up to 26. The

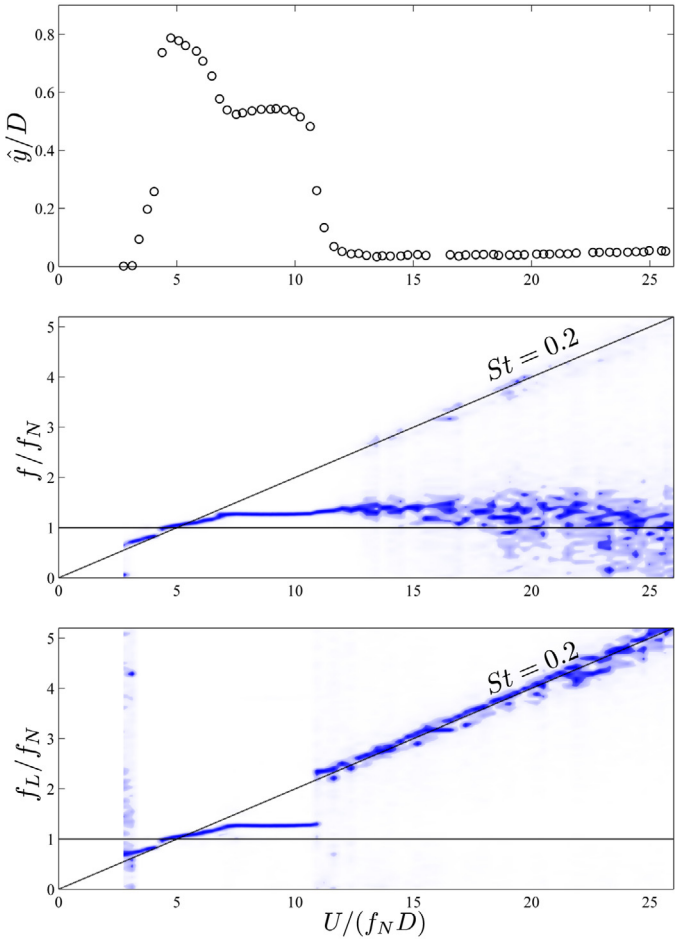

Fig. 7. (a) Amplitude of displacement, (b) spectrum of displacement and (c) spectrum of lift for a bare cylinder responding to VIV.

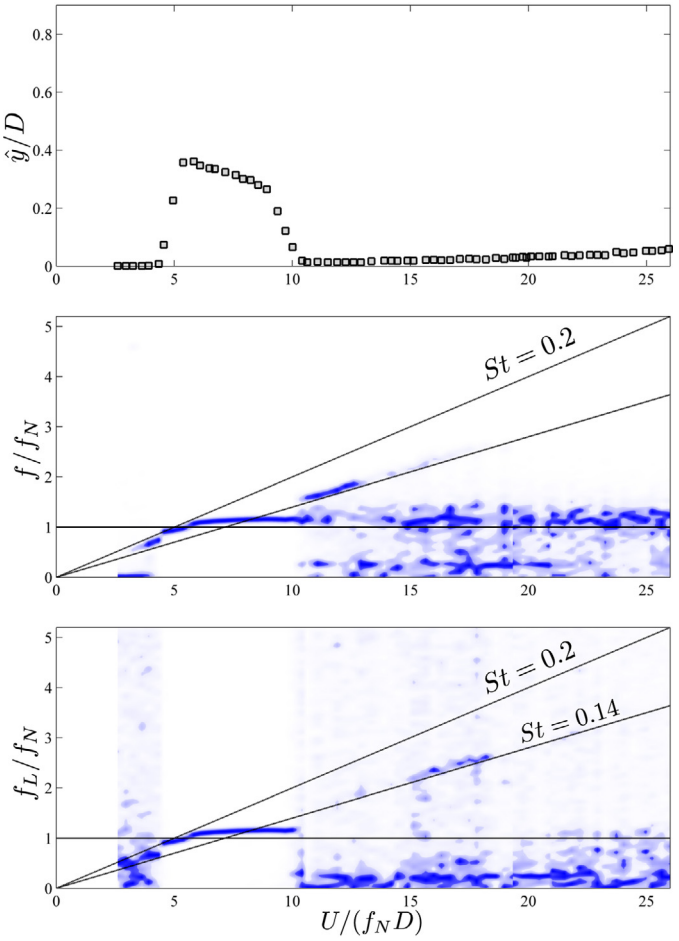

Fig. 8. (a) Amplitude of displacement, (b) spectrum of displacement and (c) spectrum of lift for a cylinder fitted with the VT responding to VIV.

frequency of oscillation (f/f_N) is not shown as points representing the dominant frequency of the spectrum (as in Fig. 6), but instead it shows the whole spectrum in different shades for each reduced velocity. Darker shades of color represent higher peaks in the frequency spectrum. This way we are able to follow concurrent branches in the frequency signature that would otherwise be hidden. While the second plot (f/f_N) in Fig. 7 shows the spectrum of displacement (the response), the third plot (f_L/f_N) shows the spectrum of lift (the excitation).

The spectrum of f/f_N shows a clear branch of dominant frequency during the synchronization range (between $U/(f_N D) = 5$ and 11), which is then dispersed in a much broader signature with no dominant frequency at the end of resonance. One may note that the bare cylinder is vibrating with very small amplitudes of displacement in a broader range of frequencies close to the natural frequency. This is a typical indication of turbulence buffeting. A faint frequency branch is barely noticeable matching the $St = 0.2$ line, which is reminiscent of the vortex shedding that is now occurring from the almost-static body. The same branch can be traced in the f_L/f_N plot, showing that at the end of the synchronization the vortex shedding mechanism returns to its "natural" regime. The magnitude of lift due to vortex-shedding, though, is not strong enough to overcome the damping of the system, that responds predominantly by buffeting.

We shall now perform the same analysis for the models with flexible shrouds. Fig. 8 shows the results for the VT, again showing a synchronization range until reduced velocity 10. Both spectra for displacement and lift show a clear dominant peak during resonance. For higher reduced velocities the spectrum of f/f_N reveals that the small vibrations are around the natural frequency, while no clear branch of lift is distinguishable, again a clear indication of turbulence buffeting. A different faint branch is noticeable in both spectra, revealing the predominant frequency of vortex shedding for the static cylinder with the VT to be lower than that of the bare cylinder. The resulting St was calculated to be approximately 0.14, which is in good agreement with Fig. 5b. (Please bear in mind that very low frequencies in the spectrum plots represent low-frequency drifts of the cylinder.)

The frequency signature for the thick-sparse mesh is presented in Fig. 9. Similarly, the synchronization range is clearly identified in both spectra, but with a little shift towards higher reduced velocities when compared to the bare cylinder (as explained before). The residual low-amplitude vibrations at higher reduced velocities is due to turbulence buffeting. This time, the frequency branch representing the vortex shedding frequency for a static model results in $St = 0.13$, as expected from Fig. 5b.

Now, the models fitted with thin meshes are the ones with a different behavior. The frequency signature for the thin-sparse mesh is

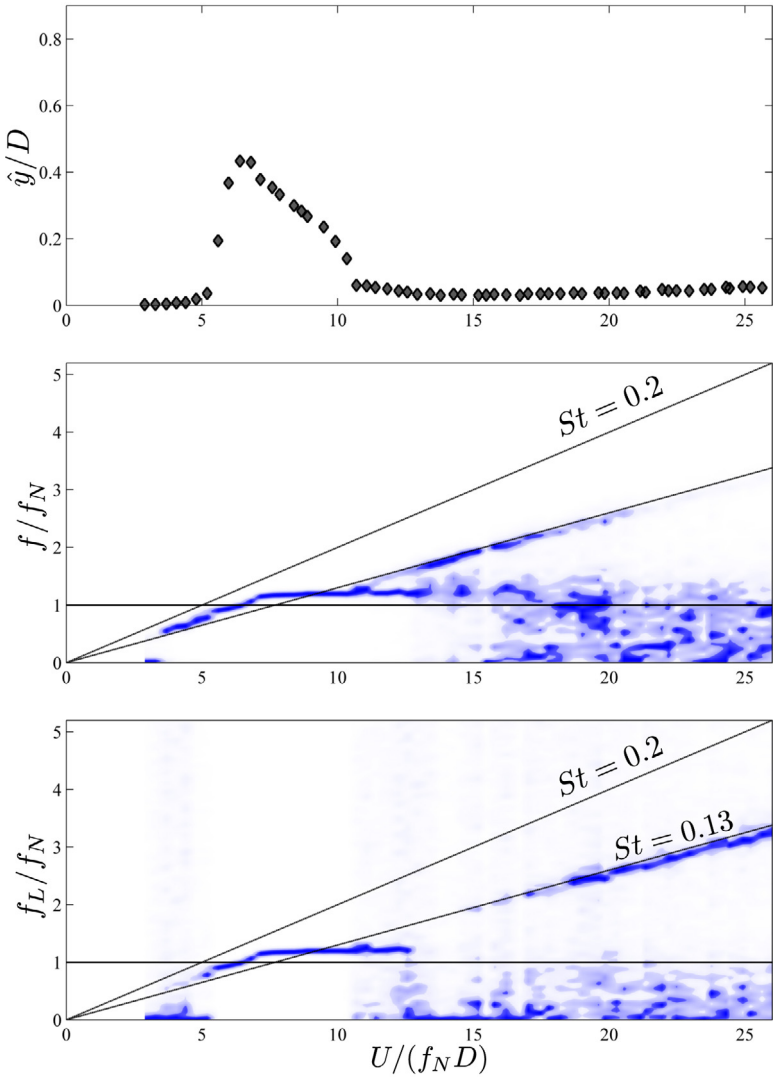

Fig. 9. (a) Amplitude of displacement, (b) spectrum of displacement and (c) spectrum of lift for a cylinder fitted with the thick-sparse mesh responding to VIV.

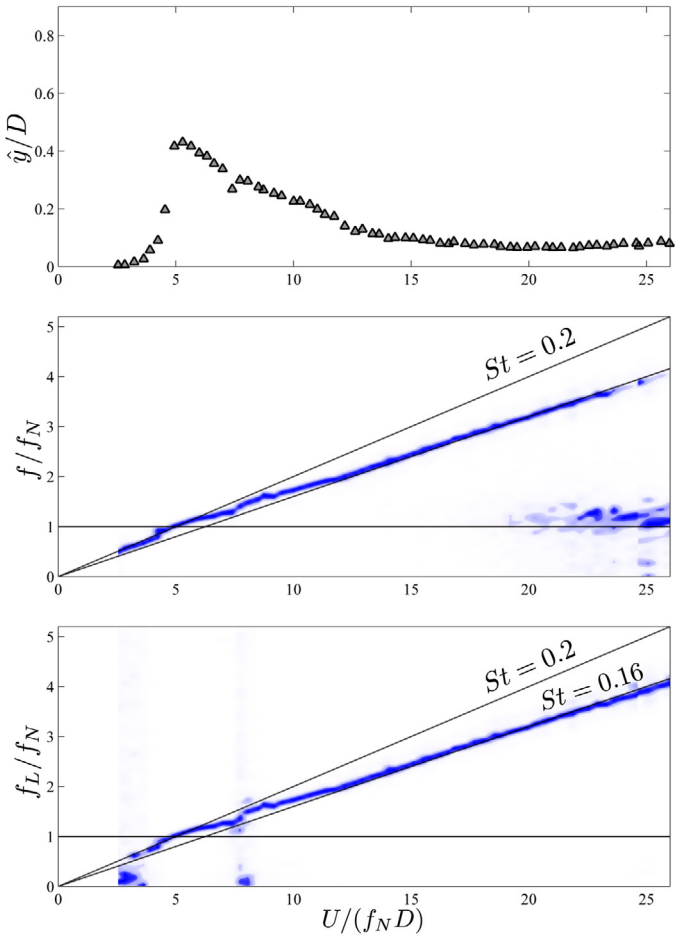

Fig. 10. (a) Amplitude of displacement, (b) spectrum of displacement and (c) spectrum of lift for a cylinder fitted with the thin-sparse mesh responding to VIV.

shown in Fig. 10. This time, the spectrum of f/f_N shows a clear branch of response following the vortex-shedding frequency. The same branch is identified in the spectrum of the excitation in f_L/f_N, yielding $St = 0.16$ for the thin-sparse mesh as in Fig. 5b. The fact that the shedding frequency is not locked-in by the oscillation frequency is rather curious. A clear resonant peak is evident in the displacement curve, but the typical synchronization range expected for classical VIV is seen not to be occurring. A region of scattered f/f_N around the natural frequency reveals the presence of turbulence buffeting for higher reduced velocities. In fact, as shown by the points of dominant frequency in Fig. 6b, both mechanisms of buffeting and harmonic vortex excitation are competing throughout the whole range of reduced velocities.

The behavior for the thin-dense mesh is similar, but intensified (Fig. 11). The spectrum of f/f_N shows a single dominant branch following the $St = 0.16$ line, also evident from f_L/f_N. St for both thin meshes are very similar because the effective diameters of the bodies are the same. The clear difference lies in the $\hat{y}/D$ curve showing that the cylinder with a thin-dense mesh shows no sign of reducing the amplitude of vibration for higher reduced velocities. Again, a non-negligible amplitude of $\hat{y}/D \approx 0.3$ is observed to occur until the end of the experiment. The cylinder does not present turbulence buffeting, but a prominent vortex-excitation mechanism dominates over the response.

As mentioned before, the clearance between the model and the thin meshes allows them to oscillate independently of the motion of the cylinder, showing movements similar to a sail. The thin-sparse mesh is as loose as the thin-dense mesh. Nevertheless, the increased number of bobbins might make the thin-dense mesh just dense enough to reduce its permeability to the flow, interact with the wake and capture more energy from the vortices. Consequently, the vortex-excitation mechanism dominates over turbulence buffeting for the whole range of reduced velocities.

Once more, it is worth highlighting that the thin meshes were seen to oscillate from side to side (more or less like a sail) as the cylinder responded to VIV. We believe this phenomenon is not much different from the hydrodynamic mechanism driving the oscillations of a cylinder fitted wit a long splitter plate (with low friction) that is free to rotate around the body, as presented by Assi et al. [13].

4. Investigation of the wake

Particle image velocimetry (PIV) measurements of the wakes have been taken for static models at $Re = 9000$. A horizontal plane illuminated the flow at mid length of the models. Two cameras were positioned side by side below the test section in order to compose a vector field wide enough to evaluate the larger flow structures in the wake. Instantaneous velocity fields were taken at a rate of 15 vector fields per second, thus producing a time-resolved analysis of 300 vector fields with almost 20 snapshots for each cycle of vortex shedding (considering f_s of the bare cylinder). Fig. 12 presents velocity vectors and vorticity contours for all the models except the thick-sparse mesh. The dashed white circle represents the masked region shadowed by the meshes. Each image is a composition of at least five instantaneous fields phase-averaged in time.

Fig. 12a shows that the bare cylinder is shedding a typical Karman wake of vortices with two single vortices per cycle. On the other hand, Fig. 12b reveals a different vortex shedding behavior for the cylinder with VT. Coherent vortex structures are indeed present in the wake, but vortices form much further downstream of the cylinder. Fig. 12c and d shows that, although the wakes of the cylinder with thin-sparse mesh and thin-dense mesh are affected by the presence of the flexible shrouds, the overall vortical structures are much more similar to that of the bare cylinder rather than that of the VT.

Examining the mean flow averaged in time from 300 images, presented in Fig. 13, one may note that the cylinder with VT (Fig. 13b) produces an extended region of velocity deficit near the base of the cylinder. Again, the mean flow in the wake of the cylinder fitted with the thin-sparse and thin-dense meshes are not much different from that in the wake of the bare cylinder.

From Figs. 12 and 13 we can conclude that the shrouds are not preventing the formation of a wake with organized vortices. They do not work to streamline the body either. In fact, a Karman wake associated with the typical flow around bluff bodies is clearly identified for all cases. The flexible shrouds do not prevent the communication of the separated shear layers, hence they are able to disrupt and modify the wake formation mechanism, but not to eliminate it altogether.

In Fig. 14 we have a quantitative view of how the wake is being modified. Measurement of the vortex-formation length are presented with streamlines of the mean flow. The color contours represent the fluctuation of the cross-flow component of velocity in the wake (v_{rms} is the root-mean-square of v, normalized by the maximum value obtained in the whole field). The locus of maximum velocity fluctuation defines the vortex formation length (L_F) indicated by a white target in each figure.

Fig. 14a shows that the Karman wake for the bare cylinder has a vortex formation length of $L_F/D = 1.5$, in agreement with the literature (please note that L_F is strongly dependent on Re [17]). Fig. 14c and d shows that the vortex formation lengths in the wake produced by the thin-sparse and thin-dense meshes

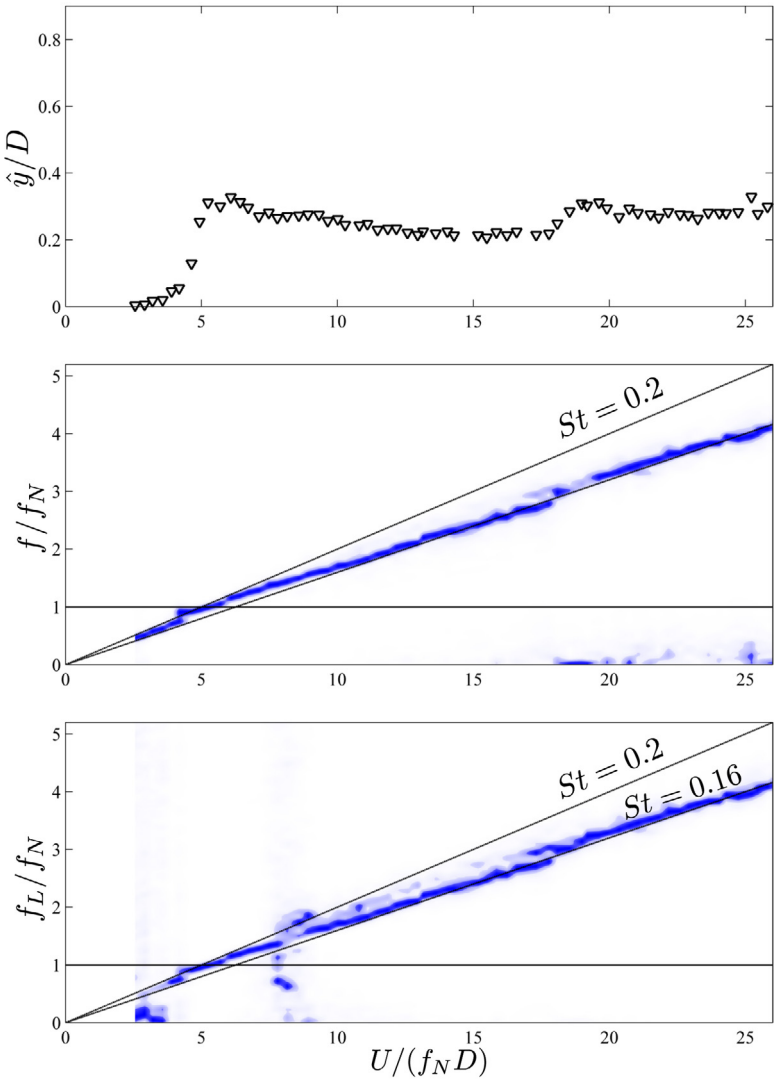

Fig. 11. (a) Amplitude of displacement, (b) spectrum of displacement and (c) spectrum of lift for a cylinder fitted with the thin-dense mesh responding to VIV.

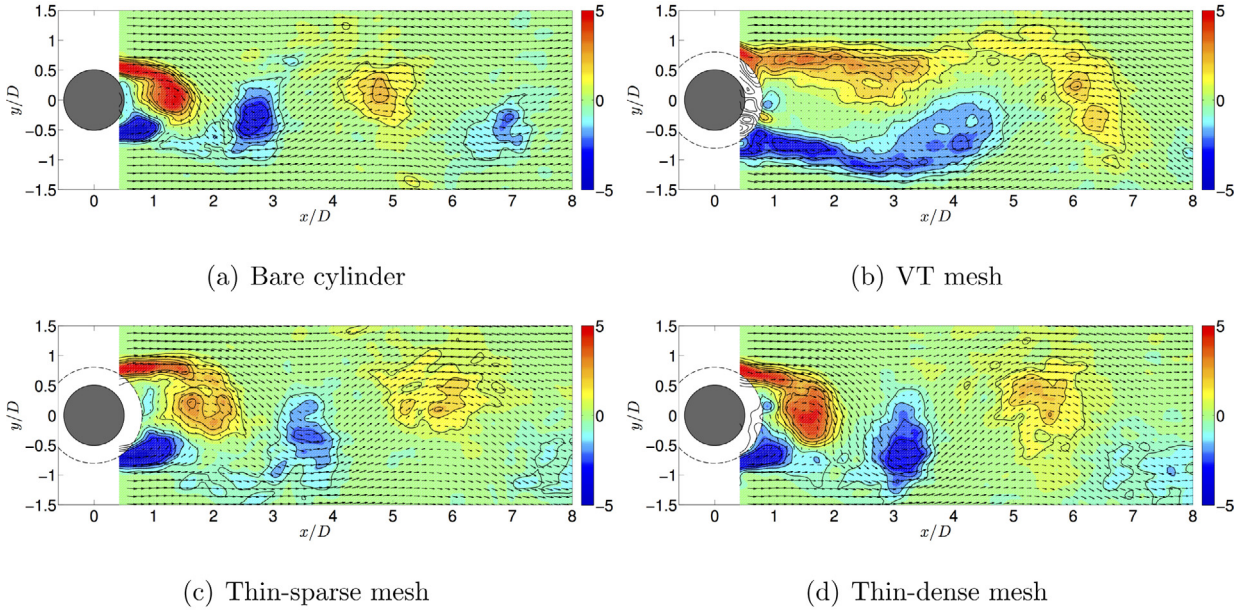

Fig. 12. Instantaneous velocity vectors and vorticity contours colored by vorticity magnitude (unit is 1/s). (a) Bare cylinder. (b) VT mesh. (c) Thin-sparse mesh. (d) Thin-dense mesh.

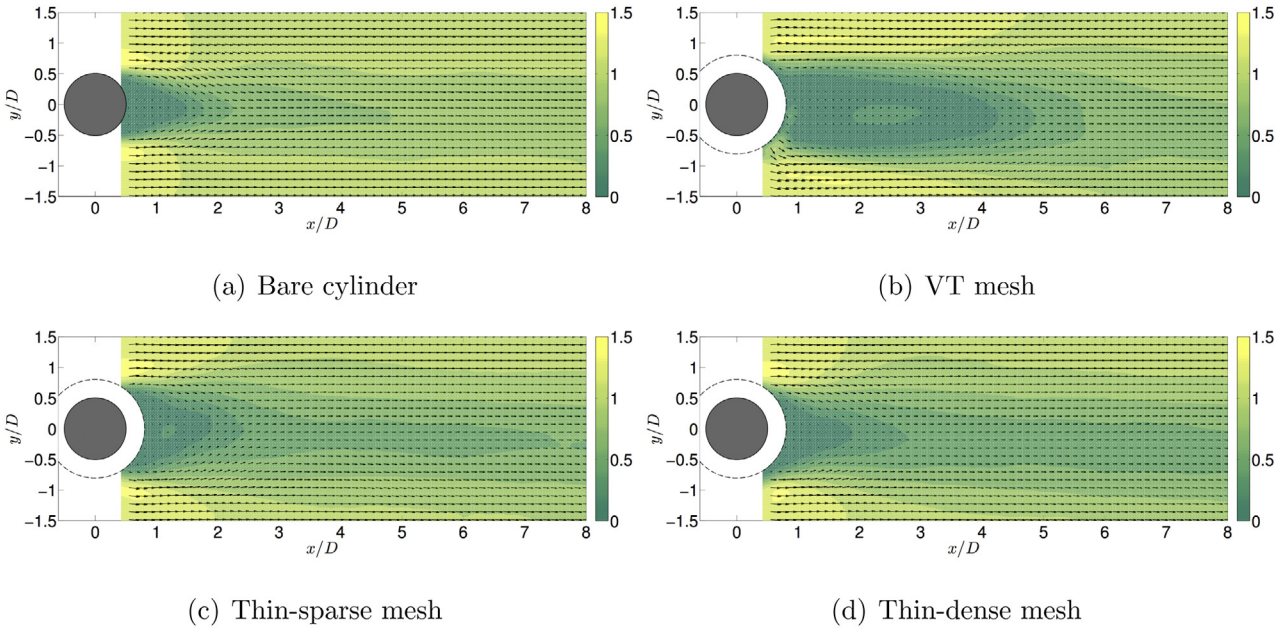

Fig. 13. Mean velocity field colored by velocity magnitude (normalized by U). (a) Bare cylinder. (b) VT mesh. (c) Thin-sparse mesh. (d) Thin-dense mesh.

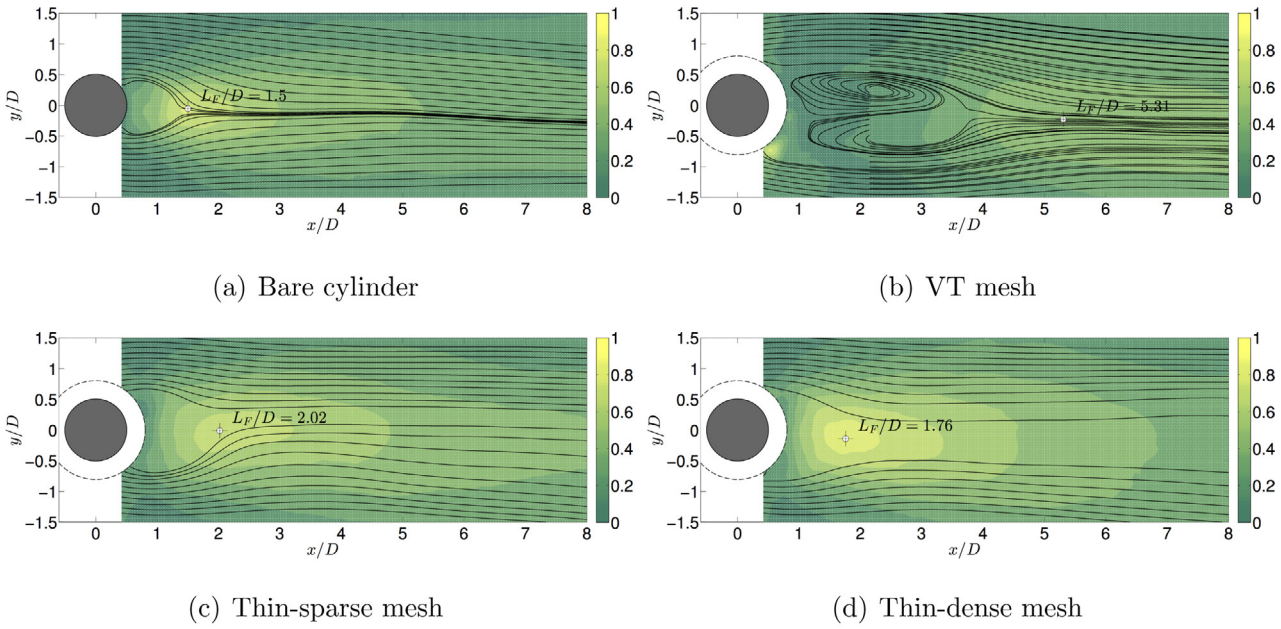

Fig. 14. RMS of the cross-flow component of velocity. v_{rms} is normalized by the maximum value found in each field. (a) Bare cylinder. (b) VT mesh. (c) Thin-sparse mesh. (d) Thin-dense mesh.

are not very different from that of the bare cylinder, being respectively $L_F/D = 2.02$ and 1,76. The case for the VT, however, shows a completely different behavior. Fig. 14b reveals a much longer vortex formation length of $L_F/D = 5.31$ in the wake of the VT.

We argue that the longer formation length found for the VT is responsible for a decrease in the fluctuating lift feeding back to excite the cylinder into VIV. A longer L_F is also related to a decrease in the mean drag. Therefore, while most of the flow is separated from the outer surfaces of the bobbins, the entrainment of flow that permeates the VT mesh bleeds through to feed the near wake region, extending the vortex-formation length and increasing the base pressure (thus reducing drag). This mechanism, illustrated in Fig. 15, is only possible due to the peculiar geometry of the VT bobbins, which is not matched by the other meshes. The outer ring of the VT bobbin separates the vertical cylindrical elements from the wall of the main cylinder, allowing for entrained fluid to flow through the mesh.

Please be aware that the PIV measurements have been performed for static cylinders in order to investigate the dominant flow structures produced by the flexible shrouds. We understand that the wake dynamics for the oscillating cylinders could be quite different from the results presented in this section. Nevertheless, the investigation of the wakes of static models has already clarified some interesting points regarding the underlying hydrodynamic mechanisms.

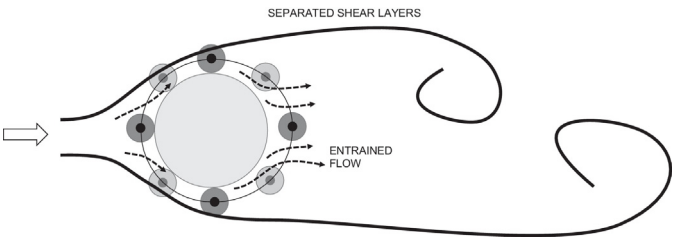

Fig. 15. Illustration of the flow around the VT mesh.

5. Concluding remarks

The preliminary experiments with fixed models revealed that all meshes increase drag for a static body. This is expected, since al meshes enlarge the area exposed to the flow and $\bar{C}_D$ is obtained using just the diameter D of the bare cylinder. The thick-sparse mesh, for instance, increases more than 30% the frontal area compared to that of the bare cylinder. Besides that, the net and bobbins increase significantly the surface area and, consequently, the friction drag. The effect of an enlarged body is also responsible for reducing the Strouhal number of the shrouds, verified in Fig. 5b.

The fluctuation of lift presented in Fig. 4 reveals that the VT and the thick-sparse mesh reduce $C_L{}'$ to values close to zero. Since the integral force is acquired at the top of the models, it is reasonable to infer that the meshes could either mitigate the sectional force, or uncorrelate lift along the span of the cylinder, or both. The most surprising result for the fixed-models experiments was the mean lift different from zero for the thin meshes. During the tests, it was verified that the meshes oscillated like a sail, breaking the body symmetry and generating a net lift force.

Observing the decay tests (Table 2), all five models have practically the same values of m^* and ζ_{air}, hence the different behaviors are related to hydrodynamic effects. From the decay tests in still water, it is verified that all models increased the hydrodynamic damping and the effective added mass. It is known that there is a strong relationship between a decrease in the peak response and an increase in $m^*\zeta$ [18,19]. Fig. 6 shows that all meshes reduced the peak response, and part of this suppression could be credited to the increase of hydrodynamic damping generated by the shrouds. On the other hand, an increase of hydrodynamic damping must not be solely the only mechanism responsible for all the suppression. For instance, the VT presents lower ζ_{water} than the thick-sparse mesh, but it is more efficient in suppressing the peak amplitude of response. As a conclusion, the geometry of the bobbin is significant, since it produces a particular change in flow, leading to different responses.

The spectrum of the VT (Fig. 8) shows that the VT is more efficient in disrupting the wake than the other meshes. After the synchronization range, the oscillation frequency of the VT remains close to f_N while the f_L shows no clear trace. The thick-sparse mesh, on the other hand, even for very small oscillations, shows a typical trace of the Strouhal frequency for both oscillation and lift frequencies. This indicates that, in spite of reducing the oscillations, the thick-sparse mesh does not eliminate coherent vortex-shedding, while the VT disrupts it better. Since their distribution is the same, the differences between the two meshes can be attributed to their bobbin geometry.

As seen from the fixed-models experiments, the thin meshes had a distinctive behavior, showing a fashion for oscillating as a sail with the wake independently of the motion of the cylinder. As shown in Figs. 6, 3(c) and (d), there is no clear synchronization range because these models always oscillate in the same frequency of vortex-shedding. In the case of thin-dense mesh, not only the oscillation continues for higher reduced velocities, but it also reaches another peak of response around reduced velocity of 20, which indicates the system is excited by another resonant frequency. The sail effect made the thin meshes extract more energy and in a wider range of frequencies than a mesh tightly attached to the cylinder; this mechanism is not associated with pure VIV.

This sail effect occurs because there is a larger clearance between the loose, thin meshes and the cylinder. Since the VT and the thick-sparse mesh have wider bobbins, their clearance is lower and the sail effect was not observed. In previous studies, Brown and King [7] noted the possibility of a "tail effect" due to the influence of mesh perimeter for VIV suppression. In the same work, they recommend a maximum value of $\frac{3}{2}\pi D$ for this parameter. As it happened, all meshes in the present study have the same perimeter, which was below that limit. Therefore we suggest that the clearance is more relevant to predict the sail phenomenon rather than the perimeter itself (because it considers the influence of bobbin size).

The only difference between the thin-sparse and the thin-dense meshes is the bobbin distribution. The thin-sparse mesh extract less energy from the flow. Therefore, we may conclude that the hydrodynamic permeability of the mesh as well as the alternating distribution of the bobbins are important parameters (the latter due to the loss of three-dimensional correlation along the span).

PIV investigation of the wake for static models revealed that the cylinder fitted with the VT mesh produces a larger vortex-formation length, indeed much larger than that for the bare cylinder. We believe the suppression efficiency of the VT is related to the weakening of the feedback mechanism of the fluctuating lift force associated with vortex shedding. We have proposed that the entrainment of the flow between the bobbins and the wall that feeds through to the near wake is necessary to extend the vortex-formation length. This mechanism is only possible to occur with the VT mesh.

Finally, it is worth highlighting that these experiments have been conducted at relatively low mass-damping systems in order to enhance the vibration. We are not saying that all devices will present the same suppression efficiency at higher *Re*, or in systems with higher damping. Experiments in an idealized laboratory condition with a rigid cylinder, with low-$m^*\zeta$, restricted to oscillate in one degree of freedom, will serve to establish the basic working principles of this family of suppressors and offer guidelines for further development.

Acknowledgements

MMC is thankful to the support of ANP Brazilian Agency of Petroleum, Natural Gas and Biofuels. GRSA is grateful to FAPESP (2011/00205-6, 2014/50279-4), CNPq (306917/2015-7) and the Brazilian Navy.

References

[1] M. Tognarelli, S. Taggart, M. Campbell, Actual VIV fatigue response of full scale drilling risers: with and without suppression devices, in: Proceedings of the 27th International Conference on Ocean, Offshore and Arctic Engineering (ASME-OMAE 2008), 2008, p. 57046.
[2] S. Taggart, M. Tognarelli, Offshore drilling riser VIV suppression devices – what's available to operators? in: Proceedings of the 27th International Conference on Ocean, Offshore and Arctic Engineering (ASME-OMAE 2008), 2008, p. 57047.
[3] G.R. Assi, P.W. Bearman, M.A. Tognarelli, On the stability of a free-to-rotate short-tail fairing and a splitter plate as suppressors of vortex-induced vibration Ocean Eng. 92 (2014) 234–244, http://dx.doi.org/10.1016/j.oceaneng.2014.10.007.
[4] M. Silva-Ortega, G. Assi, Flow-induced vibration of a circular cylinder surrounded by two, four and eight wake-control cylinders, Exp. Therm. Fluid Sci. 85 (2017) 354–362, http://dx.doi.org/10.1016/j.expthermflusci.2017.03.020.
[5] A. Brown, Device and Method for Suppressing Vortex-Induced Vibrations, Tech. Rep., United States Patent Application Publication; 2010.

[6] R. King, A. Brown, H. Braaten, M. Russo, R. Baarholm, H. Lie, Suppressing full scale riser VIV with the VT suppressor, in: Proceedings of the 32nd International Conference on Ocean, Offshore and Arctic Engineering (ASME-OMAE 2008), 2013, p. 11642.
[7] A. Brown, R. King, Tests with flexible quasi-fairing to reduce riser drag, suppress VIV and limit drilling down-time, in: Offshore Technology Conference (OTC 2008), 2008, p. 19161.
[8] M. Cicolin, C. Freire, G. Assi, VIV response and drag measurements of circular cylinders fitted with permeable meshes, in: A.S. of Mechanical Engineers (ASME) (Ed.), 34th International Conference on Ocean, Offshore and Arctic Engineering (OMAE 2015), 2015, p. 42278.
[9] M. Cicolin, Suppression of the Vortex-Induced Vibration of Circular Cylinders With Permeable Meshes (Master's thesis), Escola Politécnica, University of São Paulo, 2015, Available in Portuguese from www.teses.usp.br.
[10] G.R.S. Assi, P.W. Bearman, B.S. Carmo, J.R. Meneghini, S.J. Sherwin, R.H.J. Willden, The role of wake stiffness on the wake-induced vibration of the downstream cylinder of a tandem pair, J. Fluid Mech. 718 (2013) 210–245, http://dx.doi.org/10.1017/jfm.2012.606.
[11] M. Zdravkovich, Review and classification of various aerodynamic and hydrodynamic means for suppressing vortex shedding, J. Wind Eng. Ind. Aerodyn. 7 (1981) 145–189.
[12] M. Zdravkovich, Flow Around Circular Cylinders: Vol. 1 – Fundamentals, 1st ed., Oxford Science Publications, 1997.
[13] G.R.S. Assi, P.W. Bearman, N. Kitney, Low drag solutions for suppressing vortex-induced vibration of circular cylinders, J. Fluids Struct. 25 (2009) 666–675.
[14] C. Williamson, Three-dimensional wake transition, J. Fluid Mech. 328 (1996) 345–407.
[15] C. Norberg, Fluctuating lift on a circular cylinders: review and new measurements, J. Fluids Struct. 17 (2003) 57–96.
[16] C. Williamson, R. Govardhan, Vortex-induced vibrations, Annu. Rev. Fluid Mech. 36 (2004) 413–455.
[17] M.F. Unal, D. Rockwell, On vortex formation from a cylinder. Part 1. The initial instability, J. Fluid Mech. 190 (1988) 491–512, http://dx.doi.org/10.1017/S0022112088001429.
[18] R. Govardhan, C. Williamson, Defining the modified Griffin plot in vortex-induced vibration: revealing the effect of Reynolds number using controlled damping, J. Fluid Mech. 561 (2006) 147–180.
[19] P.W. Bearman, Vortex shedding from oscillating bluff bodies, Annu. Rev. Fluid Mech. 16 (1984) 195–228.